Conjugate Cooling Method and Application of Phase Change Material Combined with Pre-cooling of Building Envelope : Method and Model development

*Yuan Yanping**[1] *Gao Xiangkui*[1] *Wu Hongwei*[2] *Zhang Zujin*[1] *Cao Xiaolin*[1] *Yu Nanyang*[1]

[1]School of Mechanical Engineering, Southwest Jiaotong University, 610031 Chengdu, China

[2]Department of Mechanical and Construction Engineering, Faculty of Engineering and Environment, Northumbria University, Newcastle upon Tyne, NE1 8ST, United Kingdom

Abstract: In some special circumstances such as building envelope, Traditional cooling methods can not meet the requirements of safety, stability, reliability and energy saving. In Part I of this study, a new conjugate cooling method of Phase Change Material (PCM) combined with Pre-cooling of Building Envelope (PBE) is proposed and the numerical model of PBE are developed. In the current study, a refuge chamber is selected as a case study. A semi-analytical method is used to analyze the cold storage performance of the surrounding rock (SR). Afterwards, a numerical simulation model of the coupling cooling system, which take the heat source, SR, PCM and air heat transfer into consideration, is further established. The study identified that the simplified semi-analytical calculation formula with the diagram of the cold storage quantity of SR are very helpful for engineering calculation. The influence of the Fourier and Biot number on the cold storage capacity of SR can be easily analyzed. In addition, the whole-field model of the conjugate cooling system is completely developed based on the PCM unit. Part II will involve a parametric assessment and the optimization of the conjugate colling method will be explored.

Key words: phase change material; building envelope; latent heat thermal energy storage; cold storage; cooling method

Research Highlights

1. A new conjugate cooling method that combines PCM with precooling the building envelope is proposed.

2. This method can be applicable to a high-temperature and no-power circumstance.

4. The simplified calculation formula of the cold storage quantity of SR is given.

5. An efficient simulation model of the conjugate cooling system is established.

1. Introduction

Nowadays, there still exist some special spaces with high temperature and in most situations the electric power supply breakdown in Aircraft, defense engineering, mine refuge and some other facilities. Generally in such environment they have similar thermal environment and cooling demand.

Fig.1. Arrangement of permanent refuge chamber.

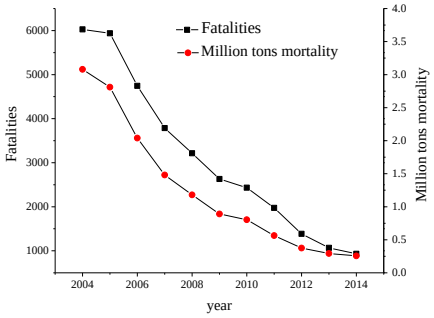

Fig.2. Fatalities and million tons mortality of mine accidents in China in 2004-2014[3].

As shown in Fig.1, the underground mine refuge chamber is the most important emergency rescue shelter [1], which provides sufficient time for the trapped miners to wait for the rescue. Such refuge chambers are sealed ones that are made of steel, which can prevent high temperature, harmful gas and shock from outside. They should providebreathable air, food, water and a safe

environment for up to hours. Thus, the refuge chamber is isolated from the mine environment without any power supply. In recent years, in the United States, South Africa and other major coal producing countries, the average annual fatalities of the coal mine is around 20 [2],while it is 1,000 in China, as illustrated in Fig.2[3]. In order to save the lives of miners, Chinese government states that the refuge chambers or other emergency rescue shelters must be installed in all mines.

Refuge chambers will be hot and humid, depending on the internal as well as the environmental conditions. As a consequence, the cooling demand in mine refuge chamber is very crucial. Van et al. [4] pointed out that when a person entered an airtight room, the indoor temperature would rise rapidly, leading to human body injury, or even death if it is not cooled within a long time. Morevoer, all power must be swiched off when the gas (coal dust) explosion occurs in a coal mine, in this case the cooling system should keep working without external power supply. In China, the refuge chamber must meet the requirement that the temperature should not exceed 35℃ within 96 hours without any external power supply.

The traditional cooling methods [5] consists of CO_2 phase change cooling, the explosion proof electrical air conditioning, the ventilation cooling and the ice storage cooling.

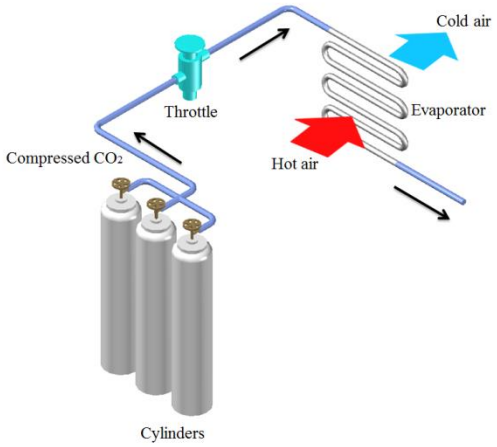

Fig.3. Schematic of CO_2 phase change cooling system.

CO_2 phase change cooling system [24], as illustrated in Fig. 3, is mainly used in the United State and Australia. But in China, it is not feasible due to the risk of leakage. In an accident, once the CO_2 leakage occurred in the mine, it would cause a large number of casualties. In order to meet the national standards requirements, the CO_2 cylinders must be inspected, maintained or replaced every year. Meanwhile, the following deficiencies of CO_2 phase change cooling system should be noticed:

i. If the ambient temperature is higher than 31 ℃, the refrigeration capacity would rapidly decrease or even disappear because the critical temperature of CO_2 is 31 ℃;

ii. The CO_2 cylinders occupy space for the large usage of CO_2;

iii. The CO_2 exhausted to the environment will affect the process of rescue.

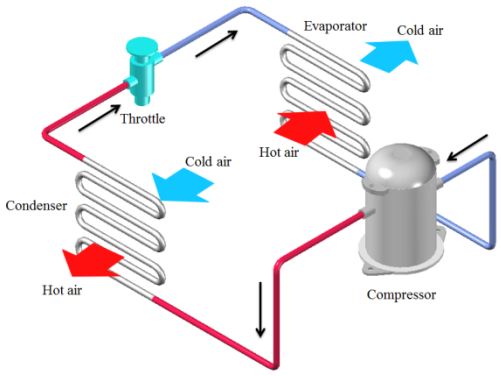

Fig. 4. Schematic of explosion proof air conditioning system.

The explosion proof air conditioning system, as illustrated in Fig. 4, is mainly used in South Africa, the United States and other countries for its excellent refrigerating effect and convenient adjustment. However, the air conditioning system would stop working when the gas explosion occurs. It is noted that Brick et al. [7] pointed out that the system must be equipped with a high capacity battery to run due to power outages caused by unexpected accidents. Currentlyand the Chinese government states that the power supply under coal mine must be intrinsically safe.

Ventilation cooling is the way to carry fresh air to the chamber through the preembedded ventilation duct or the ground drilling hole. This method can achieve the purposes of cooling and purification of indoor air in closed environments. Now it is widely used in South Africa and some other countries in numerous shallow coal mines, where the ground drilling can directly reach the refuge chamber. However, it is not suitable for China to use the ventilation cooling where the depth of mines is mainly distributed in 450~500 m. The reasons are analyzed as follows [5]:

i. The damaged probability of the ventilation duct is very high in the deep mine when mine disaster occurs, and it is expensive to use ground drilling method;

ii. The air will gradually heat up due to the effects of the air-wall convection, so it is difficult to cool the refuge chamber.

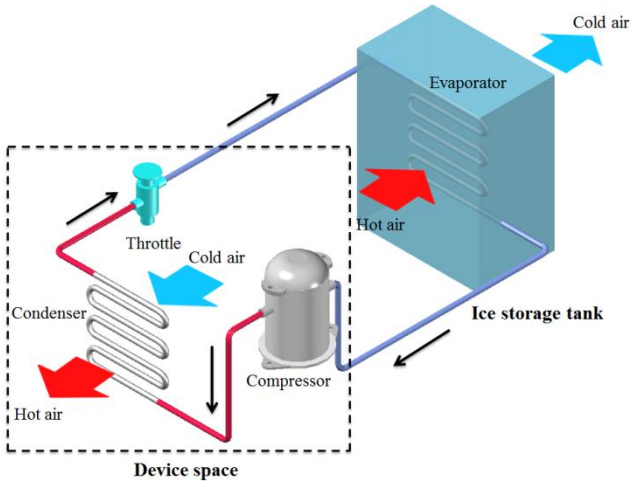

Fig. 5. Schematic of ice storage cooling.

Ice storage cooling is normally used the latent heat of the ice to cool the refuge chamber [8]. The main components of the ice storage cooling system are the device space and the ice storage tank, as shown in Fig. 5.

Ice storage cooling is a cooling concept based on PCM, which belongs to the latent heat thermal energy storage (LHTES). The LHTES system has been recently attracted an increasing interest due to their advantages such as constant temperature during phase change and high storage density [9]. Using the PCM envelope or PCM heat exchanger to control the indoor temperature is a passive temperature control method. The multi-layer PCM wallboard[10] or composite-PCM wall[11] could effectively reduce the energy demand in summer and the indoor temperature fluctuation in winter. Wang et al. [12] experimentally studied the effective thermal conductivity of composite-PCM wall. Their results showed that the effective thermal conductivity was directly proportional to the temperature in both the solid and liquid phases. During phase transition, the effective thermal conductivity varied inversely with the temperature. The combination of the PCM with floor [13] or roof [14] could also increase the thermal comfort and reduce the indoor load. Besides, using PCM heat exchanger to store natural cold and cool the room during daytime in summer is also a good way. Hed et al [15] designed a PCM-air heat exchanger. The PCM crystallized and energy was released during night, while the PCM melted and energy was stored to cool the room during daytime. Zhao et al. [16] developed a new type of shell-and-tube latent heat storage unit with fins using two heat transfer fluids (water and air). Water was used at night for energy release and air was used at daytime for energy storage. Their experimental result showed that the new air conditioning system was more applicable in charging and discharging process of

PCM. By combining the PCM heat exchanger with the ground source heat pump [17] or the solar energy system [18], the system could effectively control the temperature of the greenhouse. Kooli et al. [19] studied the temperature control system that combined phase change heat exchanger and solar energy, their experimental result showed that the indoor temperature could still be guaranteed at 15 ℃when the outdoor temperature dropped to 8 ℃ at night. Najjar et al. [20] used the enthalpy method to establish the model of the temperature control in the greenhouse, and the results showed that the temperature of the greenhouse with PCM unit can reduce 3~5 ℃ during daytime.

Ice storage cooling method is mainly used in China and because of the advantages of good security, high refrigeration efficiency and wide applicability. However, the ice storage cooling system has a serious drawback in the compressor. Namely, it is easily damaged or eroded after long time storage due to the high concentration of dust and high humidity in the mine environment. Apart from this, there are other defects:

i. Since the melting point of ice is 0 ℃, the refrigeration is needed to maintain the ice phase;

ii. Device space and ice storage tank take up large valuable living space;

iii. The fan is needed to carry the cold air to living space.

Table 1 summarized the existing cooling methods with both advantages and disadvantages in practical application.

Table 1. Evaluation and application of four cooling methods.

cooling methods	advantages	disadvantages	application
CO_2 phase change cooling	No need of electric power; Stability	The risk of leakage; Regular inspection and replacement are needed; The difficulty to maintain	Where the ambient temperature is below 31 ℃
Explosion proof air conditioning	Excellent cooling effect; Convenient adjustment	The refrigerator may not work when the gas explosion occurs; Intrinsically safe high power battery is needed	Metallic/ nonmetallic Mine
Ventilation cooling	No safety hazard; With air purification function	Ventilation ducts may be damaged; Poor cooling effect in a deep buried depth	Shallow mine
Ice storage cooling	No safety hazard; Stability	Compressor is easily eroded; High maintenance cost;	Any conditions

	Taking up large valuable living space; The fan is needed

It appears from the previous investigations that the existing cooling methods have their own application scopes and limitations and research aforementioned mainly paied attention to the improvement of thermcomfort and energy conservation of LHTES used in conventional buildings. To the best of the authors' knowledge, however, the application of LHTES in some special space such as emergency rescue shelter and military protection have been far from eomplete and there is still much room to be enhanced in this area. As such, in order to solve the problem of cooling in such special space, a new conjugate cooling method of PCM combined with PBE is proposed, which utilizes the energy storage capacity of building envelope and LHTES,. A refuge chamber in mine is selected as a case study, a series of effective system models are established to solve the thermal performance of the surrounding rock (SR) and the conjugate cooling system. For the heat transfer model of SR, a new and simple analytical solution is given, followed by a semi-analytical calculation method and the simplified calculation formula of cold storage of SR . Finally, for heat transfer the model of conjugate cooling system, the whole-field model is developed into a model based on the PCM unit.

2. Coupling cooling method and system

2.1. Congugate cooling method

As previously discussed, among the above four cooling methods, the ice storage cooling, which belongs to the LHTES, has the most important advantage requiring no electric power. In order to make LHTES system achieve better application, some improvements have been made:

i. The normal temperature PCM (such as 20℃) is selected to reduce high maintenance cost;

ii. The PCM is encapsulated into a variety of devices (such as seats) placed in the refuge chamber, in this case, the living space is saved and fan is not necessary;

iii. In a high-temperature mine, the surrounding rock can be changed from a heat source into a cold source by precooling. In this way, the surrounding rock can bear numerous indoor loads to reduce the amount of PCM. More importantly, precooling the surrounding rock can expand the

operating temperature range of PCM, which could improve the efficiency and application of PCM.

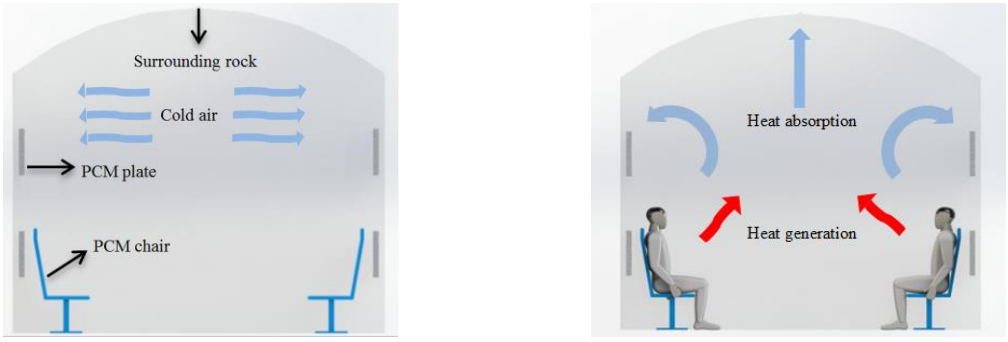

a. PBE in peacetime

b. Heat storage of PCM and building envelope during working time

Fig.6. Schematic of the coupling cooling method of PCM combined with PBE.

Based on the improvements listed above, the current work presents a conjugate cooling method of PCM combined with PBE. The basic principle is that, as shown in Fig. 6a, the building is precooled by forced-air in peacetime and the PCM at suitable temperature are encapsulated into units that placed in the building to store cold; as shown in Fig. 6b, fully using sensible heat storage capacity of building envelope and latent heat storage capacity of PCM can control the temperature during working time.

The new proposed conjugate cooling method can not only expand the operating temperature range of PCM, but also numerous cold loads to reduce the amount of PCM. It should be pointed here that the LHTES system can also be used to control the indoor temperature in a passive, stable and safe way in the harsh environment.

2.2. Introduction of coupling cooling system

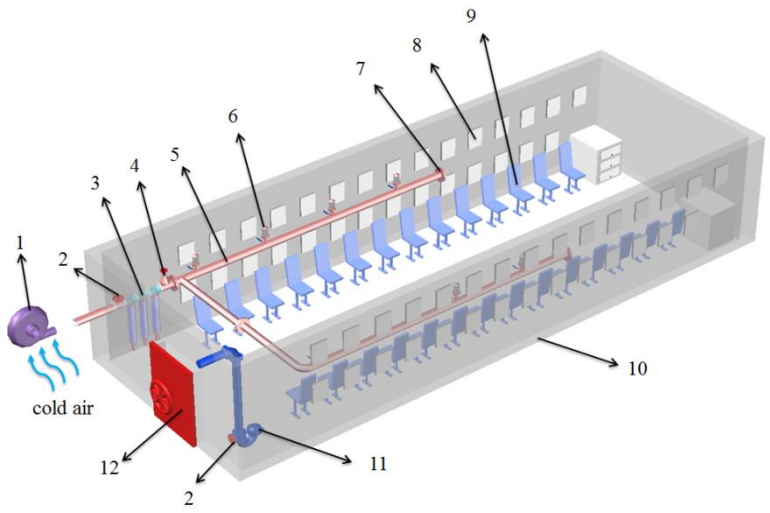

1- fan 2-valve 3- triple filter 4- pressure reducing valve 5- air pipe 6- air outlet with a silencer 7- flange 8- PCM plate 9- PCM seat 10- surrounding rock 11- automatic pressure relief valve 12- airtight door

Fig. 7. Schematic diagram of conjugate cooling system of PCM combined with PBE.

The main components of the conjugate cooling system consists of cold source, fan, air pipe, air outlet, automatic pressure relief valve and phase change cooling device, as illustrated in Fig. 7.

In precooling process, the cold air driven by fan flows through the valve, the triple filter, the pressure relief valve, the air outlet and finally into the room to precool the refuge chamber by using the ventilation duct system in the refuge chamber. When the indoor pressure is greater than the set value, the automatic pressure relief valve will open discharge part of the air to ensure that the indoor pressure is in a normal range. The fan stops running when the precooling process is completed.

If the mining area has natural cold source, such as low-temperature water (the water temperature is less than 15 ℃), cold air (winter), snow or ice, it should be fully utilized. When the natural cold source can not meet the precooling demand, the cold air should be partly shunted into the refuge chamber from the mining working face.

Intermittent cold storage technology can be used since the thermal diffusivity of the rock is small and there is no heat source in the room and convection between surrounding rock and air can be ignored. As a consequence, the indoor temperature could not have a remarkable rise during a rest period.

PCM at a room temperature be selected and encapsulated into plates hanging on the wall or seats arranged in the refuge chamber. When the indoor temperature is above the melting point, it can automatically work and does not occupy the living space.

2.3. The extended application of conjugate cooling method

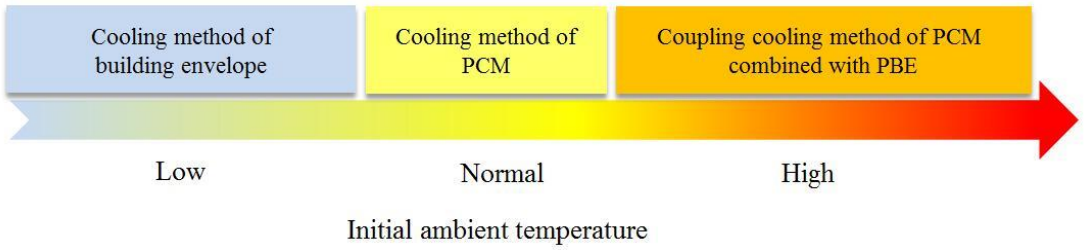

Fig. 8. The extended application of conjugate cooling method

at different initial ambient temperature.

It is noted that the initial temperature of the building envelope can directly affect the indoor load. For example, the smaller the initial temperature of the building envelope, the smaller the indoor load. Therefore, the coupling cooling method of PCM combined with PBE can be applied in different ways at different initial ambient temperature, as demonstrated in Fig. 8.

(1) Cooling method of building envelope: when the building is at a low temperature some shallow emergency rescue shelters or military protection projects, the indoor heat can be fully absorbed by building envelope. This implies that the indoor temperature will meet the needs for survival within 96 hours without the precooling process and the addition of PCM.

(2) Cooling method of PCM: when the building is at a room temperature, such as? such as some normal buried emergency rescue shelters or military protection projects, the indoor heat can not be fully absorbed by building envelope, but the indoor temperature can still meet the needs for survival by adding PCM, which means only the addition of PCM is needed in this cooling method.

(3) Coupling cooling method of PCM combined with PBE: when building is at a high temperature or a small operating temperature range condition, such as some deep buried emergency rescue shelters or military protection projects, the indoor heat cannot be absorbed by building envelope, even adding the PCM. Under this circumstance, the precooling is also needed not only to expand the operating temperature range of PCM, but also to bear numerous indoor loads.

3. Semi-analytical calculation of cold storage capacity of SR

In this section, the heat transfer of SR is calculated by using analytical method. Then the calculated results are numerical calculation method. Finally, the governing equations of cold storage capacity are derived for engineering purposes.

3.1. Governing equations and boundary conditions

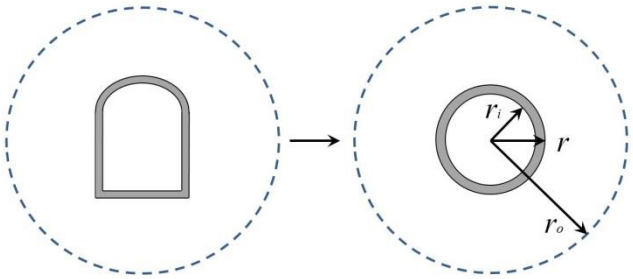

Fig. 9. Schematic of simplified structure of mine refuge chamber.

The following major assumptions for a mine refuge chamber are employed in the derivation of the governing equations [21-22]:

(i) The embedded depth of the refuge chamber is over 200 m;

(ii) The ratio of the length to the width is more than 2 and the chamber is assumed to be a cylinder, as shown in Fig. 9. $r_i=\sqrt{S/\pi}$,where， S is the area of arched section;

(iii) The heat conduction along the depth are assumed to be negligible due to its small temperature gradient;

(iv) The heat transfer caused by the moisture transfer through the rock is negligible in the present study;

(v) The thermophysical property of the SR is assumed to be constant.

Other simplifications are described in the dure course in the rest of the paper.

The equation for calculating the changes in the temperature of SR in vector form is:

$$\frac{\partial t}{\partial \tau}=a\frac{\partial^2 t}{\partial r^2}+\frac{1}{r}\cdot\frac{\partial t}{\partial r} \tag{1a}$$

$$-\lambda_w\frac{\partial t(r_i,\tau)}{\partial r}=h_w\left[t_f-t(r_i,\tau)\right] \tag{1b}$$

$$t(r_o,\tau)=t_0 \tag{1c}$$

$$t(r,0)=t_0 \tag{1d}$$

where t_0 is the initial temperature, τ is the time, a is the the thermal diffusivity, r is the radius of the SR, r_i is the inner wall radius, λ_w is the thermal conductivity, t_f is the air temperature, r_o is the outer surface radius. h_w is the natural convective heat transfer coefficient between the air and inner wall, which is calculated by the Eq. (2) [23]:

$$h_w=6.76\times v^{0.8}+0.74 \tag{2}$$

3.2. Analytical solution of heat conduction equation

Taking $\theta=t-t_f$, the Eq. (1) can be converted into Eq. (3):

$$\frac{\partial\theta}{\partial\tau}=a\left(\frac{\partial^2\theta}{\partial r^2}+\frac{1}{r}\cdot\frac{\partial\theta}{\partial r}\right) \tag{3a}$$

$$\lambda\frac{\partial\theta(r_i,\tau)}{\partial r}=h_w\theta(r_i,\tau) \tag{3b}$$

$$\theta(r_o,\tau)=\theta_o \tag{3c}$$

$$\theta(r,0)=\theta_o \tag{3d}$$

This equation can be described by Eqs. (4) and (5) following the method of linear superposition.

$$\frac{\partial^2\theta_1}{\partial r^2}+\frac{1}{r}\cdot\frac{\partial\theta_1}{\partial r}=0 \tag{4a}$$

$$\lambda\frac{\partial\theta_1(r_i,\tau)}{\partial r}=h_w\theta_1(r_i,\tau) \tag{4b}$$

$$\theta_1(r_o,\tau)=\theta_o \tag{4c}$$

$$\frac{\partial\theta_2}{\partial\tau}=a\left(\frac{\partial^2\theta_2}{\partial r^2}+\frac{1}{r}\cdot\frac{\partial\theta_2}{\partial r}\right) \tag{5a}$$

$$\lambda\frac{\partial\theta_2(r_i,\tau)}{\partial r}=h_w\theta_2(r_i,\tau) \tag{5b}$$

$$\theta_2(r_o,\tau)=0 \tag{5c}$$

$$\theta_2(r,0)=\theta_o-\theta_1(r) \tag{5d}$$

Eq. (4) is an ordinary differential equation and can be solved as:

$$\theta_1(r)=\theta_0\cdot\frac{1+\dfrac{h_w r_i}{\lambda}\ln\dfrac{r}{r_i}}{1+\dfrac{h_w r_i}{\lambda}\ln\dfrac{r}{r_o}} \tag{6}$$

Eq. (5) can be solved by the method of separation of variables. Taking $\theta_2=R(r)T(\tau)$, the Eq. (5) can be converted into :

$$\frac{T'}{aT}=\frac{rR''+R'}{rR}=-\eta \tag{7}$$

where, η is a positive constant. Let $\eta=\beta^2$, the Eq. (7) can be rewritten as:

$$T'+a\beta^2T=0 \tag{8a}$$

$$r^2R''+rR'+r^2\beta^2R=0 \tag{8b}$$

The general solution of Eq. (8a) is:

$$T(\tau)=Be^{-a\beta^2\tau} \tag{9}$$

where, B is a constant..

Eq. (8b) is a standard zero order Bessel equation and the general solution is given by:

$$R(r)=CJ_0(\beta r)+DY_0(\beta r) \tag{10}$$

where, C and D are constants, J_0 and Y_0 areclass I and II Bessel functions of the zero order respectively. According to the liner superposition principle, the solution of Eq. (5) can be expressed as:

$$\theta_2(r,\tau)=Be^{-a\beta^2\tau}\left[CJ_0(\beta r)+DY_0(\beta r)\right] \tag{11}$$

With the boundary conditions of Eq. (5c), the solution of Eq. (8b) can be written as:

$$R(r)=Y_0(\beta r_o)J_0(\beta r)-J_0(\beta r_o)Y_0(\beta r) \tag{12}$$

With the boundary conditions of Eq. (5b), the Eq. (11) can be converted into Eq. (13) following the recursion formulae of Bessel functions.

$$\frac{Y_0(\beta r_o)J_1(\beta r_i)-J_0(\beta r_o)Y_1(\beta r_i)}{Y_0(\beta r_o)J_0(\beta r_i)-J_0(\beta r_o)Y_0(\beta r_i)}=-\frac{h_w}{\lambda\beta} \tag{13a}$$

where, J_1 and Y_1 areclass I and II Bessel functions of the first order, respectively. And Eq. (13a) can be simplified as:

$$E_1(\beta r_i) = E_2(\beta r_i) \tag{13b}$$

where, $E_1(\beta r_i)=[Y_0(\beta r_o)J_1(\beta r_i)-J_0(\beta r_o)Y_1(\beta r_i)]\beta r_i$, $E_2(\beta r_i)=[Y_0(\beta r_o)J_0(\beta r_i)-J_0(\beta r_o)Y_0(\beta r_i)]Bi$, $Bi=h_w r_i/\lambda$.

Eq.(13b) is a transcendental equation, which can be solved by graphic method.. The infinite intersections of the two curves are the characteristic roots β_m and the corresponding characteristic function is $R_0(\beta_m r)= Y_0(\beta_m r_o)J_0(\beta_m r)-J_0(\beta_m r_o)Y_0(\beta_m r)$.

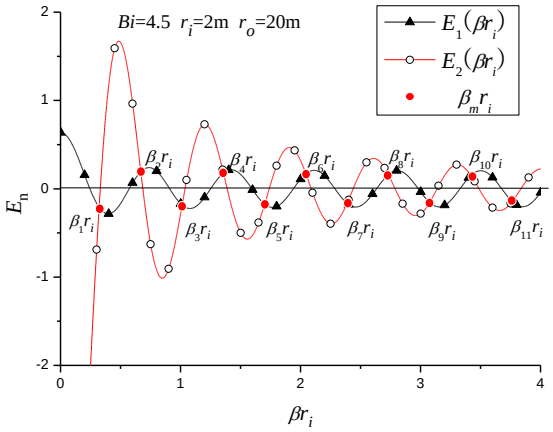

Fig.10. Solving process of β_m.

The solution of Eq. (8) is given by:

$$\theta_2 = \sum_{m=1}^{\infty} B_m e^{-a\beta_m^2 r} R_0(\beta_m r) \tag{14}$$

The equation Eq. (14) is multiplied by $rR_0(\beta_n r)$ and then integrate r in $[r_i, r_o]$. According to the theory of Sturm-Liouville [24], the characteristic function $R_0(\beta_m r)$ and $R_0(\beta_n r)$ is orthogonal in the interval when $\beta_m \neq \beta_n$. So Eq.(14) can be rewritten as:

$$\int_{r_i}^{r_o} rR_0(\beta_m r)[\theta_0 - \theta_1(r)]dr = B_m \int_{r_i}^{r_o} rR_0^2(\beta_m r)dr \tag{15}$$

Left side of Eq.(15) is solved by Eq.(16).

$$\int_{r_i}^{r_o} rR_0(\beta_m r)[\theta_0 - \theta_1(r)]dr = \frac{\theta_0 \dfrac{h_w r_i}{\lambda}}{1+\dfrac{h_w r_i}{\lambda}\ln\dfrac{r_o}{r_i}}\left[\frac{\ln r_o}{\beta_m}\cdot rR_1(\beta_m r)\Big|_{r_i}^{r_o} - \int_{r_i}^{r_o} rR_0(\beta_m r)\ln r dr\right]$$

$$= \frac{\theta_0 \dfrac{h_w r_i}{\lambda}}{1+\dfrac{h_w r_i}{\lambda}\ln\dfrac{r_o}{r_i}}\left\{\frac{\ln r_o}{\beta_m}\cdot rR_1(\beta_m r)\Big|_{r_i}^{r_o} - \left[\frac{r}{\beta_m}R_1(\beta_m r)\ln r\Big|_{r_i}^{r_o} - \frac{1}{\beta_m}\int_{r_i}^{r_o} R_1(\beta_m r)dr\right]\right\}$$

$$= \frac{\theta_0 \dfrac{h_w r_i}{\lambda}}{1+\dfrac{h_w r_i}{\lambda}\ln\dfrac{r_o}{r_i}}\left[\frac{r_i \ln\dfrac{r_i}{r_o}}{\beta_m}\cdot R_1(\beta_m r_i)+\frac{1}{\beta_m^2}R_0(\beta_m r_i)\right] \tag{16}$$

where, $R_1(r)= Y_0(\beta r_o)J_1(r)- J_0(\beta r_o)\, Y_1(r)$， $R_0(r)= Y_0(\beta r_o)J_0(\beta r)- J_0(\beta r_o)\, Y_0(r)$。

To solve the right side of Eq. (15), the equation Eq. (8b) is multiplied by $rR_0'(\beta_m r)$ and then integrate r in $[r_i, r_o]$. The result can be seen in Eq. (17d).

$$\int_{r_i}^{r_o}\left(rR_0'\right)\left(rR_0'\right)'dr+\int_{r_i}^{r_o} r\beta_m^2 R_0\left(rR_0'\right)dr=0 \tag{17a}$$

$$\frac{1}{2}\left(rR_0'\right)^2\Big|_{r_i}^{r_o}+\beta_m^2 r^2\left(\frac{1}{2}R_0^2\right)\Big|_{r_i}^{r_o}-\beta_m^2\int_{r_i}^{r_o} rR_0^2 dr=0 \tag{17b}$$

$$\int_{r_i}^{r_o} rR_0^2(\beta_m r)dr=\frac{r_o^2}{2}R_1^2(\beta_m r_O)-\frac{r_i^2}{2}R_1^2(\beta_m r_i)-\frac{r_i^2}{2}R_0^2(\beta_m r_i) \tag{17c}$$

$$\int_{r_i}^{r_o} rR_0^2 dr=\frac{r_o^2}{2}R_1^2(\beta_m r_O)-\frac{r_i^2}{2}\left(1+\frac{h_w^2}{\lambda^2\beta_m^2}\right)R_0^2(\beta_m r_i) \tag{17d}$$

B_m can be solved by Eq. (15), Eq. (16), Eq. (17d).

$$B_m=\frac{\dfrac{\theta_0 \dfrac{h_w r_i}{\lambda}}{1+\dfrac{h_w r_i}{\lambda}\ln\dfrac{r_o}{r_i}}\left[\dfrac{r_i \ln\dfrac{r_i}{r_o}}{\beta_m}\cdot R_1(\beta_m r_i)+\dfrac{1}{\beta_m^2}R_0(\beta_m r_i)\right]}{\dfrac{r_o^2}{2}R_1^2(\beta_m r_O)-\dfrac{r_i^2}{2}\left(1+\dfrac{h_w^2}{\lambda^2\beta_m^2}\right)R_0^2(\beta_m r_i)} \tag{18}$$

The solution of Eq. (3) is:

$$\theta=\theta_0\cdot\frac{1+\dfrac{h_w r_i}{\lambda}\ln\dfrac{r}{r_i}}{1+\dfrac{h_w r_i}{\lambda}\ln\dfrac{r_o}{r_i}}+ \tag{19}$$

$$\theta_0\cdot\frac{\dfrac{h_w r_i}{\lambda}}{1+\dfrac{h_w r_i}{\lambda}\ln\dfrac{r_o}{r_i}}\sum_{m=1}^{\infty}e^{-a\beta_m^2\tau}R_0(\beta_m r)\frac{\dfrac{\beta_m r_i \ln\dfrac{r_i}{r_o}}{}R_1(\beta_m r_i)+R_0(\beta_m r_i)}{\dfrac{r_o^2\beta_m^2}{2}R_1^2(\beta_m r_O)-\left(\dfrac{r_i^2\beta_m^2}{2}+\dfrac{r_i^2 h_w^2}{2\lambda^2}\right)R_0^2(\beta_m r_i)}$$

Finally, the temperature contribution of SR is given by:

$$t(r,\tau)=t_f+\left(t_0-t_f\right)\cdot\frac{1+\dfrac{h_w r_i}{\lambda}\ln\dfrac{r}{r_i}}{1+\dfrac{h_w r_i}{\lambda}\ln\dfrac{r_o}{r_i}}+ \tag{20}$$

$$\left(t_0-t_f\right)\cdot\frac{\dfrac{h_w r_i}{\lambda}}{1+\dfrac{h_w r_i}{\lambda}\ln\dfrac{r_o}{r_i}}\sum_{m=1}^{\infty}e^{-a\beta_m^2\tau}R_0(\beta_m r)\frac{\dfrac{\beta_m r_i \ln\dfrac{r_i}{r_o}}{}R_1(\beta_m r_i)+R_0(\beta_m r_i)}{\dfrac{r_o^2\beta_m^2}{2}R_1^2(\beta_m r_O)-\left(\dfrac{r_i^2\beta_m^2}{2}+\dfrac{r_i^2 h_w^2}{2\lambda^2}\right)R_0^2(\beta_m r_i)}$$

where, $R_0(\beta_m r)= Y_0(\beta_m r_o)J_0(\beta_m r)-J_0(\beta_m r_o)Y_0(\beta_m r)$， $R_1(\beta_m r)= Y_0(\beta_m r_o)J_1(\beta_m r)-J_0(\beta_m r_o)Y_1(\beta_m r)$。

3.3. Determination of semi-analytical calculation parameters

Eq. (20) is an analytical solution for SR. The general behavior is given by the analytical solution turned into a complete dimensionless expression:

$$\Theta(\Gamma, Bi, Fo)=\frac{1+Bi\ln\Gamma}{1+Bi\ln\Phi}+\frac{Bi}{1+Bi\ln\Phi}\sum_{m=1}^{\infty}e^{-Fo\Psi_m^2}R_0(\Gamma\Psi_m)\frac{R_0(\Psi_m)-\Psi_m R_1(\Psi_m)\ln\Phi}{\frac{(\Phi\Psi_m)^2}{2}R_1^2(\Phi\Psi_m)-\frac{\Psi_m^2+Bi^2}{2}R_0^2(\Psi_m)} \quad (21)$$

where, $\Theta=[t(r,\tau)-t_f]/(t_0-t_f)$ is a dimensionless temperature, $\Gamma=r/r_i$ is the dimensionless radius of the depth, $Fo=a\tau/r_i^2$ is the Fourier number, $Bi=h_w r_i/\lambda$ is the Biot number, $\Psi_m=\beta_m r_i$ is the dimensionless radius of the inner wall, $\Phi=r_o/r_i$ is the dimensionless radius of far boundary. Ψ_m is a function of Γ and *Bi*.

adopted to calculate Eq. (21). Three parameters should be determined during the numerical calculation: 1.) dimensionless radius of far boundary Φ; 2.) the times of infinite sum *m* 3.) calculation accuracy A.

3.3.1. Dimensionless radius of far boundary

Φ is an important parameter for numerical calculation. If Φ becomes larger, the result can be more close to the real situation, but it will occupy too much computer resources. Therefore, the accuracy and speed of calculation should be comprised. Table 2 gives the computing parameter to calculate the influence of Φ on Θ_{ri}.

Table 2. Computing parameters of dimensionless radius of far boundary.

Symbol	Description	Value
Γ	The dimensionless radius	1
Bi	Biot number	4.5
Fo	Fourier number	∞
Φ	The dimensionless radius of far boundary	10~2000

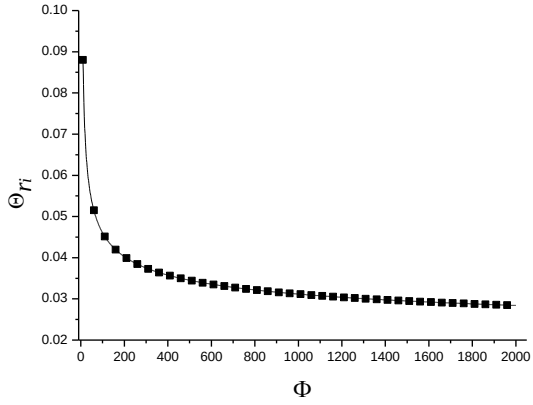

Fig.11. Influence of Φ on Θ_{ri}.

Fig.11 shows the influence of Φ on Θ_{ri}. As is expected, Θ_{ri} decreases with the increase of Φ. From Fig. 11, it can be seen clearly when Φ varies from 10 to100 and 100 to 2000, Θ_{ri} decreases 0.042 and 0.018 respectively. It is found that Φ=100 is economic with sufficient accuracy in the present study.

3.3.2. Times of infinite sum

There is an infinite sum term in Eq. (21) and the times of the infinite sum *m* should be determined priot to the real numerical calculation. The selected input data in the model are listed in Table 3.

Table 3. Computing parameters of times of sum.

Symbol	Description	Value
Γ	The dimensionless radius	1
Bi	Biot number	4.5
Fo	Fourier number	0~0.15
N	The dimensionless radius of far boundary	100
A	Calculation accuracy of Ψ_m	rounded to 4 decimal places
m	the times of infinite sum	*m*=200,400,600,800,1000

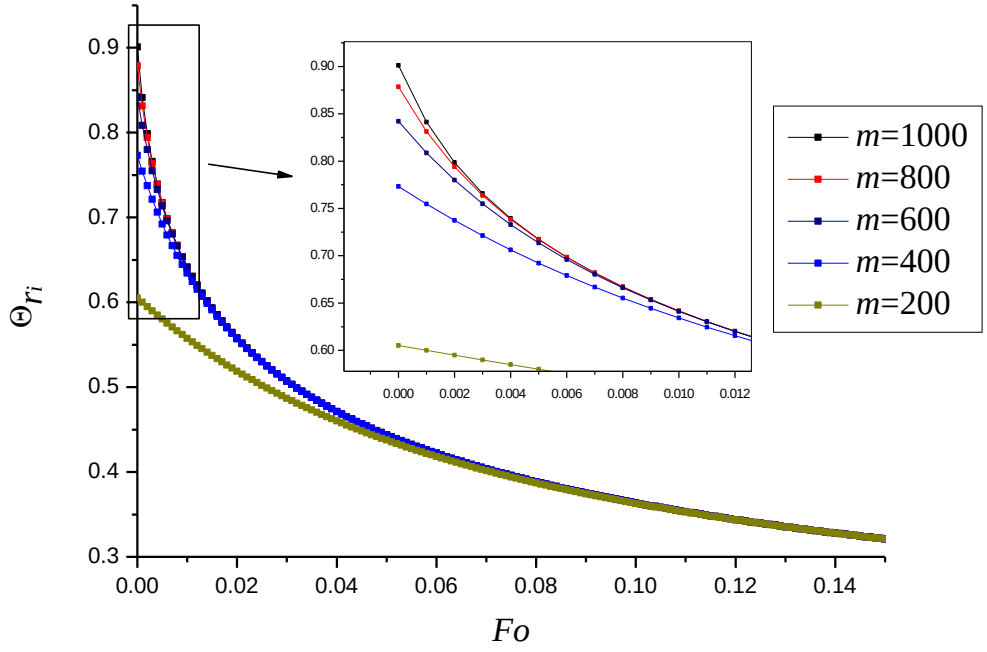

Fig.12. Θ_{ri} versus *Fo* at different *m*.

Fig. 12 shows Θ_{ri} versus *Fo* at different *m*. It can be seen clearly that the smaller the *Fo* , the greater the *m* . More concretely, *m*=800 is the suitable value when *Fo*≥0.01 and *m*=200 is the suitable value when *Fo*≥0.1.

Table 4. *m* value selected under different *Bi* and *Fo*.

Bi	*Fo*≥0.01	*Fo*≥0.1
0.3	500	180
0.5	560	180
0.7	600	200
0.9	620	200
1.0	640	200
2.0	660	220
3.0	700	240
4.0	740	260
5.0	800	260
6.0	800	260
7.0	800	260
8.0	800	260
9.0	800	260
10.0	800	260
15.0	800	260
20.0	800	260

Table 4 shows *m* value selected at different *Bi* and *Fo*. It appears that *m* increases with *Bi* and it keeps unchanged when *Bi*≥4.5. For the general type of ventilation cooling in mine refuge chamber, m=800 is suggested as the approximate calculation times of infinite sum.

3.3.3. Calculation accuracy

Ψ_m is the solution of transcendental Eq. (13b), which is solved by point by point test algorithm. The calculation accuracy for Therefore, it is necessary to select appropriate calculation accuracy. Table 5 gives the computing parameter.

Table 5. Calculation parameters of ??? of Ψ_m.

Symbol	Description	Value
Γ	The dimensionless radius	1
Bi	Biot number	4.5
Fo	Fourier number	0~0.1
N	The dimensionless radius of far boundary	100
A	Calculation accuracy of Ψ_m	rounded to 3、4、5、6 decimal places
m	times of infinite sum	800

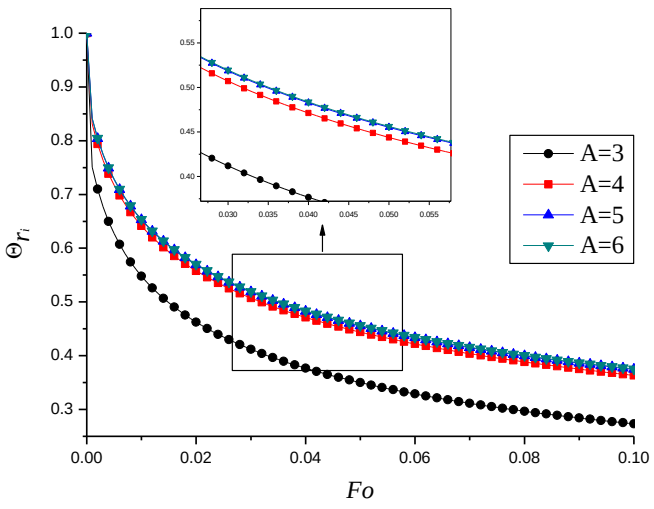

Fig.13. Θ_{ri} versus *Fo* at different A.

Fig.13 shows the calculated results at different different A, i.e. A=3, 4, 5 and 6. It can be seen clearly that the optimal value of A is

5 for the present case, also noted that the tendency is almost the same when comparing the curve at A=6. If the value of A is too low, for instance A=3, the result would change greatly.

Table 6. Computational errors of A at different *Bi*.

Bi	A=3	A=4	A=5
0.3	46.07%	0.31%	0.33%
0.5	29.50%	1.49%	0.10%
0.7	16.63%	3.06%	0.28%
0.9	38.35%	3.43%	0.42%
1.0	33.37%	3.75%	0.13%
2.0	28.14%	2.38%	0.28%
3.0	22.23%	2.81%	0.31%
4.0	17.80%	2.07%	0.22%
5.0	16.10%	2.35%	0.14%
6.0	13.59%	2.05%	0.13%
7.0	12.92%	1.75%	0.19%
8.0	12.24%	1.75%	0.12%
9.0	12.09%	2.18%	0.21%
10.0	11.07%	2.27%	0.21%
15.0	42.78%	1.89%	0.17%
20.0	9.15%	1.96%	0.14%

Table 6 shows the computational errors between A = 3~5 and A=6 at different *Bi*. It appears that the computational errors with the change of *Bi* are irregular. But different A has a different range of error values. When A varies from 3 to5, the ranges of error values are 10~40%, 1~4%, 0.1~0.4%, respectively. Therefore, A=5 is adopted for its lower computational error.

3.4. Model validation

In order to verify the semi-analytical method of computing the ventilation in tunnel, the calculated results were compared to the experimental result. Experiment was carried out in a test tunnel. The dimensions of the tunnel were 6 m (length)×0.1 m (internal diameter)×0.4 m (outer diameter). The thermal diffusivity and conductivity of SR were 0.8×10^{-6} m^2/s and 1.2 J/(m·K), respectively. Initial temperature of the tunnel was 30℃. Air supply velocity and temperature were 5 m/s and 20 ℃, respectively. The ventilation time was 3.5 h. For more details on the test tunnel and instrumentations refer to Zhang [25].

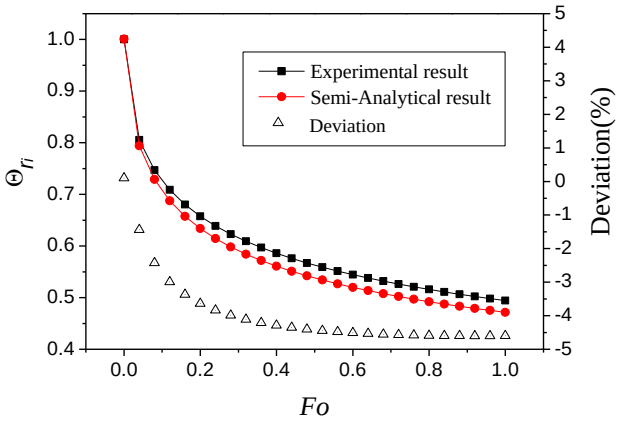

Fig. 14. Comparison of the simulated and experimental results.

Fig. 14 shows the comparison of the simulated and experimental results. And the error curve, calculated based on $\Delta\Theta_{ri}/\Theta_{ri,exp}\times 100\%$, is also shown in Fig.14. The results show that the maximum difference of Θ_{ri} was 0.025 and the deviation is less than 5%. The semi-analytical predicted result is in a good agreement with the experimental result, which shows that this method is suitable for the study in this paper.

3.5. Calculation of cold storage quantity of SR and its engineering simplification

Cold storage quantity of SR is the cold quantity stored in the SR within the scope of the heat control circle, which can determine the cold storage capacity of SR and the current cooling level.

Heat control circle r_c shows the range of SR where the temperature is changed in time τ. There is no standard definition of r_c, and the r_c is defined as Eq.(26) in the present study.

$$\frac{t_{r_c} - t_{r_i}}{t_{r_o} - t_{r_i}} = 0.995 \tag{26}$$

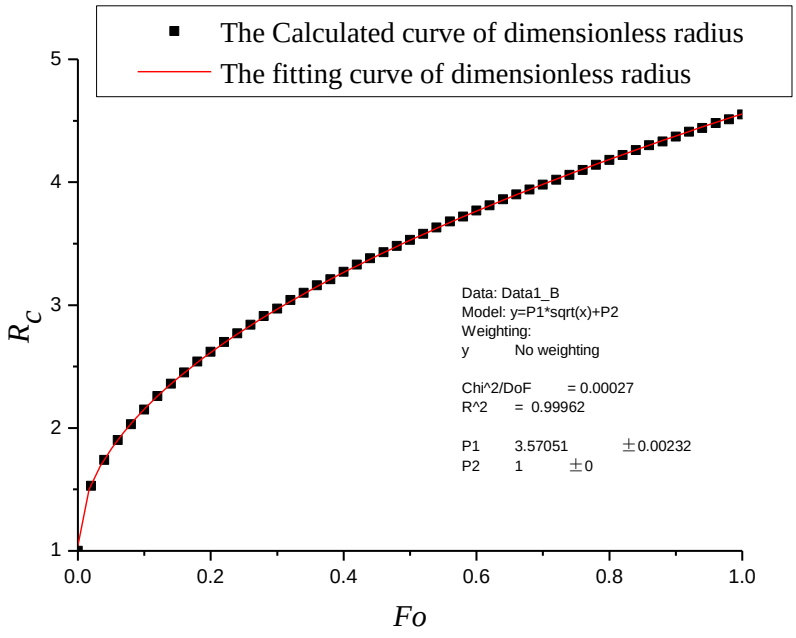

Fig.15. the dimensionless radius of r_c versus Fo and its fitting curve.

When Bi=4.5, the curve of R_c-Fo is shown in Fig. 15. Where, $R_c=r_c/r_i$ is the dimensionless radius of r_c. The fitting curve is:

$$R_c = 3.57\sqrt{Fo} + 1 \qquad R^2 = 0.9996 \tag{27}$$

With $R_c=r_c/r_i$,$Fo=a\tau/r_i^2$, the Eq. (27) can be described as:

$$r_c - r_i = 3.57\sqrt{a\tau} \tag{28}$$

Table 8. Fitting results of r_c under different Bi.

Bi	Fitting results
1.0	$r_c - r_i = 3.42\sqrt{a\tau}$
2.0	$r_c - r_i = 3.46\sqrt{a\tau}$
3.0	$r_c - r_i = 3.51\sqrt{a\tau}$
4.0	$r_c - r_i = 3.55\sqrt{a\tau}$
5.0	$r_c - r_i = 3.60\sqrt{a\tau}$
6.0	$r_c - r_i = 3.63\sqrt{a\tau}$

7.0	$r_c - r_i = 3.67\sqrt{a\tau}$
8.0	$r_c - r_i = 3.71\sqrt{a\tau}$
9.0	$r_c - r_i = 3.74\sqrt{a\tau}$
10.0	$r_c - r_i = 3.77\sqrt{a\tau}$

Table 8 shows the fitting results of r_c under different *Bi*. It can be seen that the effect of *Bi* is very small and the coefficient η is used to represent the effect in engineering calculation:

$$r_c - r_i = 3.6\eta\sqrt{a\tau} \tag{29}$$

where

$$\begin{cases} 7 \le Bi \le 14 & \eta = 1.05 \\ 3 < Bi < 7 & \eta = 1 \\ Bi \le 3 & \eta = 0.95 \end{cases}$$

Because the rated protection time of refuge chamber is 96h, the cold storage quantity is solved by integrating the temperature difference from r_i to r_c(τ=96h).

The temperature difference is:

$$\Delta t(\Gamma, Bi, Fo) = (t_0 - t_f)\left[\frac{Bi\ln\frac{\Phi}{\Gamma}}{1+Bi\ln\Phi} - \frac{Bi}{1+Bi\ln\Phi}\sum_{m=1}^{\infty} e^{-Fo\Psi_m^2} R_0(\Gamma\Psi_m) \frac{R_0(\Psi_m) - \Psi_m R_1(\Psi_m)\ln\Phi}{\frac{(\Phi\Psi_m)^2}{2}R_1^2(\Phi\Psi_m) - \frac{\Psi_m^2 + Bi^2}{2}R_0^2(\Psi_m)}\right] \tag{30}$$

Set f_1:

$$f_1 = \frac{Bi\ln\frac{\Phi}{\Gamma}}{1+Bi\ln\Phi} - \frac{Bi}{1+Bi\ln\Phi}\sum_{m=1}^{\infty} e^{-Fo\Psi_m^2} R_0(\Gamma\Psi_m) \frac{R_0(\Psi_m) - \Psi_m R_1(\Psi_m)\ln\Phi}{\frac{(\Phi\Psi_m)^2}{2}R_1^2(\Phi\Psi_m) - \frac{\Psi_m^2 + Bi^2}{2}R_0^2(\Psi_m)} \tag{31}$$

Then Eq. (30) can be written as:

$$\Delta t(\Gamma, Bi, Fo) = (t_0 - t_f) f_1(\Gamma, Bi, Fo) \tag{32}$$

The cold storage quantity Q_{SR} is:

$$Q_{SR}(Bi, Fo) = C_p\rho(t_0 - t_f)\int_{r_i}^{r_i + 2116\eta\sqrt{a}} A(r) f_1(\Gamma, Bi, Fo)dr \tag{33}$$

where, A is the area. It is too complicated to calculate Q_{SR} by using Eq. (33), and there needs to simplify it helping the engineering calculation.

$$Q_{SR}(Bi, 0) = 0 \tag{34}$$

$$Q_{SR}(Bi,\infty)=C_p\rho(t_0-t_f)\int_{r_i}^{r_i+2116\eta\sqrt{a}}A(r)\frac{Bi\ln\frac{\Phi}{\Gamma}}{1+Bi\ln\Phi}dr \quad (35)$$
$$=EC_p\rho(t_0-t_f)\int_{r_i}^{r_i+2116\eta\sqrt{a}}A(r)dr$$
$$=EC_p\rho(t_0-t_f)V_c$$

where, $V_c=\int_{r_i}^{r_i+2116\eta\sqrt{a}}A(r)dr$ is the volume of r_c. $E=\frac{\int_{r_i}^{r_i+2116\eta\sqrt{a}}A(r)\frac{Bi\ln\frac{\Phi}{\Gamma}}{1+Bi\ln\Phi}dr}{\int_{r_i}^{r_i+2116\eta\sqrt{a}}A(r)dr}$, is a simplified calculation factor, which means the ratio of Q_{SR} in a long time ($\tau\to\infty$) to Q_{SR} when temperature in SR is equal to precooling temperature.

Table 9. Calculation value of *E*.

Bi	$a=8.07\times10^{-7}$ m²/s (clay)		$a=9.06\times10^{-7}$ m²/s (Sandstone)		$a=12.8\times10^{-7}$ m²/s (gneiss)	
	r_i=1.5 m	r_i=2 m	r_i=1.5 m	r_i=2 m	r_i=1.5 m	r_i=2 m
4	0.853	0.872	0.849	0.869	0.835	0.857
5	0.862	0.881	0.858	0.878	0.844	0.866
6	0.868	0.887	0.864	0.884	0.850	0.872
7	0.872	0.892	0.868	0.889	0.854	0.876
8	0.876	0.895	0.872	0.892	0.857	0.880
9	0.878	0.898	0.874	0.895	0.860	0.882
10	0.880	0.900	0.876	0.897	0.862	0.884
11	0.882	0.902	0.878	0.899	0.863	0.886
12	0.883	0.903	0.879	0.900	0.865	0.888
13	0.885	0.904	0.881	0.901	0.866	0.889
14	0.886	0.905	0.882	0.902	0.867	0.890

Table 9 shows the influence of the thermal diffusivity *a*, the equivalent radius r_i and the *Bi* on the E value. It can be seen that the value of *E* is between 0.84 and 0.9. The influence of r_i on *E* is obvious, the bigger the r_i, the greater the *E*; The effect of *Bi* on *E* is also positively correlated; o nly the effect of a on E value is negatively correlated. Its calculation is as follows:

$$E=0.85\eta_1\eta_2\eta_3 \quad (36)$$

η_1- correction coefficient of r_i, $\eta_1=0.048r_i+0.928$

η_2- correction coefficient of *Bi*, $\eta_2=1.057-0.2Bi^{-0.9}$

η_3- correction coefficient of *a*, $\eta_3=-43950a+1.04$

With the Eq. (33)~(35), the engineering calculation formula of Q_{SR} in the range of r_c (τ=96h) is obtained:

$$Q_{SR} = EC_p\rho\left(t_0 - t_f\right)V_c \times f_2\left(Bi, Fo\right) \tag{37}$$

$$f_2\left(Bi,0\right) = 0$$

$$f_2\left(Bi,\infty\right) = 1$$

where, f_2 is the function of Bi and Fo.

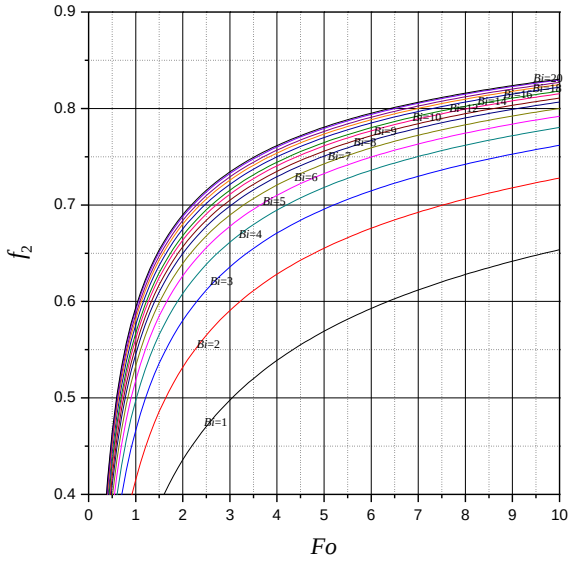

Fig. 16. Diagram of $f_2(Bi,Fo)$.

In this paper, a numerical method is used to calculate a large number of Q_{SR} values under different Bi and Fo conditions in order to help the engineering calculation, and the diagram of $f_2(Bi, Fo)$ is obtained as shown in Fig. 16.

5. Model establishment and solution of conjugate cooling system

5.1 Mathematical model

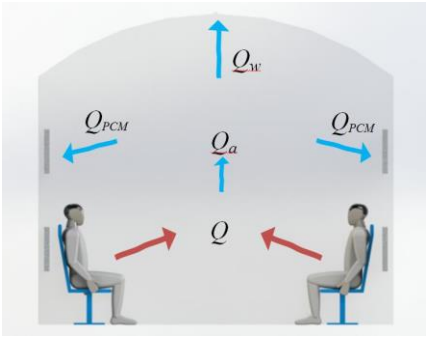

Fig.17. Schematic diagram of heat transfer of conjugate cooling system

As shown in Fig. 17, the conjugate cooling process includes the heat transfer among phase change units, surrounding rocks, air and heat sources in a closed space. In the current work, the phase change units hang on the wall with the form of plates and the back ventilation is adopted to enhance the convective heat transfer. For the purpose of convenience, the following assumptions are made:

ⅰ) Assuming that the heat source is constant and ignore the effect of radiation;

ⅱ) Neglecting the heating time of air and its temperature distribution is uniform;

ⅲ) Out of the influence of temperature fluctuation from ground surface for its embedded depth is 400~600m;

ⅳ) The material of surrounding rock is homogeneous and isotropic and neglecting the heat transfer caused by the moisture transfer through the envelope;

ⅴ) The chamber can be simplified as a cylinder and heat transfer through walls is one-dimensional [22];

ⅵ) Assuming that the thermal physical properties of PCM are constant, but it is different for solid and liquid phases. The change of the density of the fluid is considered only when the influence of the buoyancy is involved [26].

5.1.1. Heat transfer model of SR

The one dimensional heat conduction equation is the same with Eq. (1).

where the boundary conditions are

$$\begin{cases} -\lambda_w \dfrac{\partial t(r_i,\tau)}{\partial r} = h_w\left[t_f - t(r_i,\tau)\right] \\ t(r_o,\tau) = t_0 \end{cases} \tag{38}$$

with initial condition is

$$t(r,0) = t_0 \tag{39}$$

where, t_0 is the initial temperature, τ is the time, a is the thermal diffusivity, r is the radius of the SR, r_i is the inner wall radius, λ_w is the thermal conductivity, t_f is the air temperature, r_o is the outer surface radius. h_w is the natural convective heat transfer coefficient between the air and inner wall, which can be calculated by the formula (40) and (41) [27]:

$$Nu = \frac{hl}{\lambda_a} \tag{40}$$

$$Nu = 0.59(Gr\,\mathrm{Pr})^{1/4} \tag{41}$$

where, Nu is the Nusselt number, l is the feature size, λ is the thermal conductivity of air. $Gr = g\alpha_V \Delta t l^3 / \nu^2$ is the Grashof number, where g is the acceleration of gravity, α_V is the air volume expansion coefficient, Δt is the temperature difference, v is the dynamic viscosity, Pr is the Planck number.

5.1.2. *Heat transfer model of PCM plate*

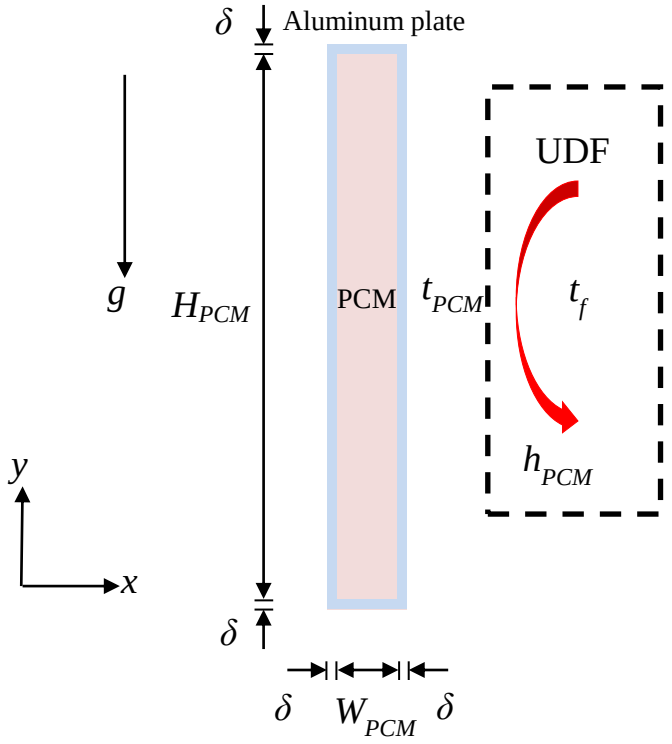

Fig. 18. Computational domain and boundary conditions at the vertical mid-plate of PCM plate

PCMs are encapsulated by aluminum plate and the thickness of the plate is 1.5 mm. The geometry of the PCM plate is designed as follows (not including the aluminum plate): the length L_{PCM} is 600 mm, the height H_{PCM} is 500 mm, and the thickness W_{PCM} is 60 mm. As shown in Fig. 18, the vertical mid-plane of the PCM plate is selected as the computational domain.

The transient enthalpy equations are [26]

$$\begin{cases} \dfrac{\partial \rho}{\partial \tau} + div\left(\rho \vec{v}\right) = 0 \\ \dfrac{\partial \left(\rho h'\right)}{\partial \tau} + div\left(\rho u u\right) = div\left(u \cdot gradv\right) - \dfrac{\partial P}{\partial x} + S_x \\ \dfrac{\partial \left(\rho h'\right)}{\partial \tau} + div\left(\rho u v\right) = div\left(u \cdot gradv\right) - \dfrac{\partial P}{\partial y} + S_y + S_b \\ \dfrac{\partial \left(\rho h'\right)}{\partial \tau} + div\left(\rho \vec{v} h'\right) = div\left(\lambda_{PCM} \cdot gradt\right) - S_{h'} \end{cases} \tag{42}$$

where, h' is the enthalpy, λ_{PCM} is the thermal conductivity of PCM, $S_x = A_{mush}\mu(1-f)^2/(f^2+\varepsilon)$ and

$S_y=A_{mush}v(1-f)^2/(f^2+\varepsilon)$ are the source terms in the fuzzy region. Where ε is a zero denominator to prevent small (ε=0.001), A_{mush} is a fuzzy area constant, set to 100000. The source term method is introduced to solve the problem of the unity of the momentum equation of the solid, liquid and fuzzy terms. $S_b=\rho g\alpha(t-t_m)$ is the Buoyancy term. Where, α=0.0005K^{-1} is the material expansion coefficient.

The relationship between the enthalpy h' and the temperature t can be expressed as follows [28]

$$h'=\begin{cases} c_p t, & t<t_s \\ c_p t+\dfrac{t-t_s}{t_l-t_s}\Delta h', & t_s\le t\le t_m \\ c_p t+\Delta h', & t>t_m \end{cases} \tag{43}$$

where, c_p is the specific heat, $\Delta h'$ latent heat, t_s solidification temperature, t_m melting temperature. The liquid phase fraction f is introduced to ensure the unity of the enthalpy equation and can be expressed as follows [19]

$$f=\begin{cases} 0, & t<t_s \\ \dfrac{t-t_s}{t_m-t_s}, & t_s\le t\le t_m \\ 1, & t>t_m \end{cases} \tag{44}$$

As a result, the enthalpy can be described as a unified form:

$$h'=c_p t+f\cdot\Delta h' \tag{45}$$

The boundary conditions are

$$\begin{cases} -\lambda_{PCM}\dfrac{\partial t}{\partial x}=h_{PCM}\left[t_{PCM}-t_f\right] \\ -\lambda_{PCM}\dfrac{\partial t}{\partial y}=h_{PCM}\left[t_{PCM}-t_f\right] \\ v=0,u=0 \end{cases} \tag{46}$$

The initial condition is

$$t(x,y,0)=t_{c0} \tag{47}$$

where, t_{PCM} is the outer surface temperature of PCM plate; h_{PCM} is the natural convection heat transfer coefficient between air and PCM plate, calculated by Eq. (40) and Eq. (41).

5.1.3. Model of indoor air

The energy conservation equation is used to calculate the temperature of the air:

$$C_a \rho_a V_a \frac{\partial t_f}{\partial \tau} = q + q_w + q_{PCM} \tag{48}$$

where, C_a is the specific heat of air; q is the indoor heat flux; q_w is the convective heat flux between air and SR; q_{PCM} is the convective heat flux between air and PCM plate. q, q_w, q_{PCM} are calculated by the following formula:

$$q = N_p q_p \tag{49}$$

$$q_w = h_w A_{i,w} \left(t_w - t_f \right) \tag{50}$$

$$q_{PCM} = N_{PCM} h_{PCM} A_{PCM} \left(t_{PCM} - t_f \right) \tag{51}$$

where, N_p is the number of people in refuge chamber; q_p is per capita heat generation rate (including equipments); $A_{i,w}$ is area of the inner wall; N_{PCM} is the the number of PCM plates; A_{PCM} is the area of the outer surface of one PCM plate.

5.2. Numerical solution method and model validation

5.2.1. Numerical solution method

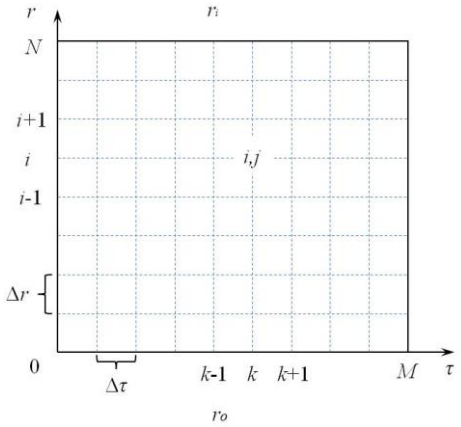

Fig.19. Computational grid of SR.

Since the temperature boundary condition of SR is affected by the conjugate cooling process, Eq. (1) is calculated by finite volume method instead of the semi-analytical method. Fig. 19 shows the computational grid of SR. The basic discrete units are:

$$\frac{\partial t}{\partial \tau}=\frac{t_i^k-t_i^{k-1}}{\Delta \tau},\quad \frac{\partial t}{\partial r}=\frac{t_{i+1}^k-t_{i-1}^k}{2\Delta r},\quad \frac{\partial^2 t}{\partial r^2}=\frac{t_{i+1}^k-2t_i^k+t_{i-1}^k}{\Delta r^2} \tag{52}$$

The discrete results of Eqs. (1), (38), and (39) are shown as Eq. (53). The temperature distribution of SR can be obtained by using the numerical calculation method.

$$\begin{cases} t_i^k=t_{c0} & i=0 \\ (\dfrac{Fo\Delta r}{2r_i}-Fo)t_{i-1}^k+(1+2Fo)t_i^k-(Fo+\dfrac{Fo\Delta r}{2r_i})t_{i+1}^k=t_i^{k-1} & i=1\sim N-1 \\ -2Fot_{i-1}^k+(1+2BiFo+2Fo)t_i^k=t_i^{k-1}+2FoBit_f & i=N \end{cases} \tag{53}$$

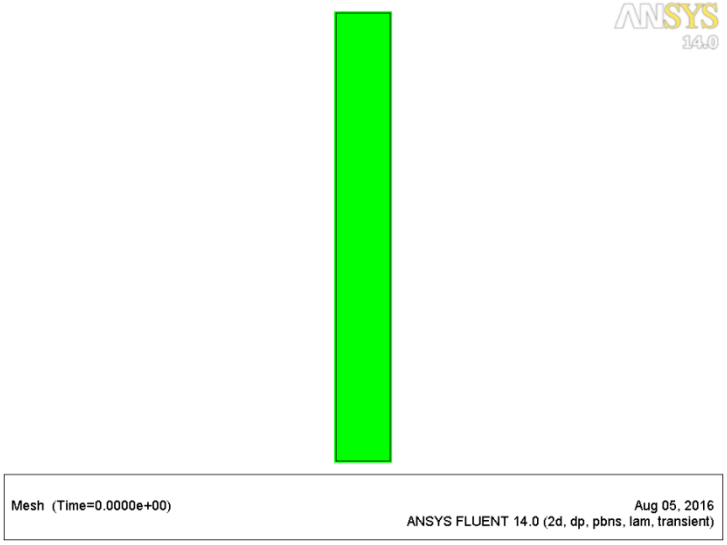

Fig.20. Computational Grid of PCM plate.

In the current suty, the heat conduction, convection and melting processes are coupled in the PCM plate, so the PCM plate model is set as the main model. The air temperature and convection heat transfer coefficient, calculated by User Defined Function （UDF）, are in the form of boundary conditions in the main model. The calculation software is ANSYS Fluent14.0. The calculation is based on the melting and solidification model. The influence of natural convection is considered in the PCM unit, and the density calculation is based on the Boussinesq assumption. The heat transfer of outer aluminum surface of the PCM plate is convection, and the convection heat transfer temperature and coefficient are t_f and h_{PCM}, respectively. The interface between the aluminum surface and the PCM is the coupled interface. The time step is 1s, and the total number of steps is 345600. Fig.20 shows the 2D computational grid of PCM plate.

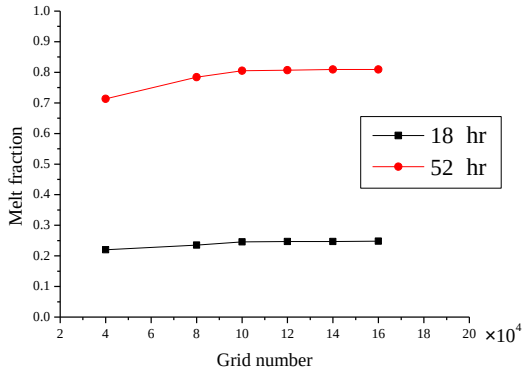

Fig. 21. Comparison of melting fraction under different grid numbers

A mesh independence study was conducted to identify an appropriate mesh density for the aimed calculations. Six meshes, 40,000, 80,000, 100,000, 120,000, 140,000 and 160,000 were investigated. Fig. 21 shows the comparison of melting fractions under six different grids. It is found that the melting fraction change has been less than 0.1% when the number of grids is 100,000, so the 100,000 grids was selected for the calculation.

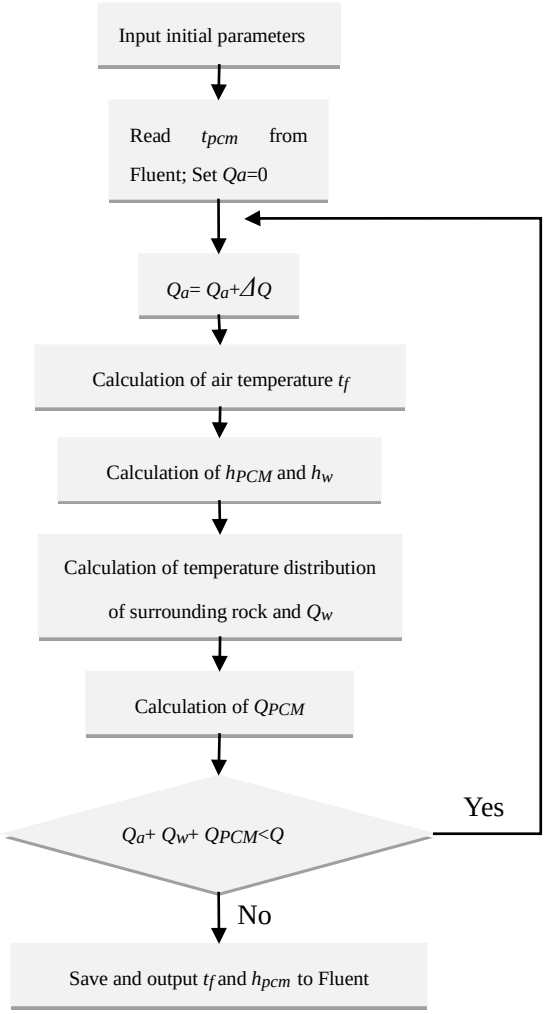

Fig. 22. Program flow chart of UDF.

The program flow chart of UDF to calculate t_f and h_{PCM} is shown in Fig. 22. The calculation process is divided into the following steps:

(1) Input initial parameters, then read t_{PCM} from Fluent and set Q_a =0, ΔQ=1W;

(2) Calculate $Q_a=Q_a+\Delta Q$;

(3) Calculate t_f with Eq. (48), then calculate h_{PCM} and h_w with Eq. (40), (41). With the calculated t_f, h_{PCM} and h_w, the temperature distribution of SR and PCM plate can be solved, and the value of Q_w and Q_{PCM} are also can be got.

(4) Determine the size of $Q_a+ Q_w+ Q_{PCM}$ and Q. If $Q_a+ Q_w+ Q_{PCM}< Q$, then turn to step (2) and calculate again; If $Q_a+ Q_w+ Q_{PCM}> Q$, stop the calculation.

(5) Save and output t_f and h_{PCM} to Fluent.

5.2.2. Model validation

In the current study, to verify the correctness of using enthalpy-porosity model to calculate the melting process, the calculated result is compared with the experimental data of Babak et al. [29]. The experiment was carried out in a rectangular device with acid lauric placed in a vertical position. One side of the aluminum plate was heated with the constant temperature of 70℃, and the other surfaces were thermal insulation surfaces. The length was 120 mm, the height was 120 mm, and the thickness was 50 mm.The initial temperature was 25℃, and 32 thermocouples were built-in to detect the temperature distribution. PCM properties can be seen in Table 10[29].

Table 10. Thermo physical properties of lauric acid.

Specific heat capacity solid/liquid	2.182.39	kJ/kg·K
Melting temperature range	43.5/48.2	℃
Latent heat of fusion	187.21	kJ/kg
Thermal conductivity solid/liquid	0.16/0.14	W/m·K
Density solid/liquid	940/885	kg/m^3
Kinematic viscosity	6.7×10^{-6}	m^2/s
Prandtl	100.7	

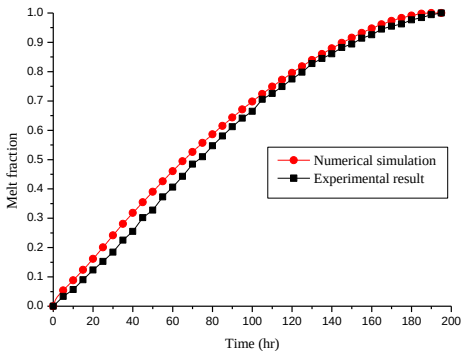

Fig. 23. Comparison of the experimental and numerical melt fractions.

Fig. 23 shows the comparison of the melt fractions between the experimental data and numerical results and close agreement is achieved. It can be seen clearly that the simulation result is a little faster than the experiment result. It is noted that the experiment uses the heat source to maintain the constant temperature, so there exists a small thermal resistance.

6. Conclusions

A new conjugate cooling method of PCM combined with PBE is proposed and the refuge chamber in mine is slected as a case study The simulation model of the whole process is developed and the governing equations are solved usingthe finite volume method. Firstly, compared the coupling cooling method with the traditional cooling method, the results show that the existing cooling methods such as CO_2 phase change cooling, the explosion proof electrical air conditioning and the ventilation cooling have their own defects in safety, no power, or stability, which is a threat to the safety of the asylum workers. Ice storage cooling method is one kind of LHTES, which does not have the above threat, but the drawbacks are also obvious, for example, the compressor is easily eroded, maintenance cost is high and so on. Apart from meeting the requirements of safety, no power, stability and reliability, the coupling cooling method also has the merits of small occupied volume, no maintenance in peacetime and fully utilization of the external natural cold source.

Secondly, semi-analytical method is used to analyze the cold storage performance of SR. By using the separation variable method, the analytical solution of heat transfer in SR is derived. Then, the simplified semi-analytical calculation formula and the diagram of the cold storage quantity of SR are given for engineering calculation. According to the diagram, the influence of *Fo* and *Bi* number on cold storage capacity of SR can be easily analyzed.

Lastly, a numerical simulation model of coupling cooling system, considering heat source, SR, PCM and air heat transfer, is established. According to respective heat transfer characteristics of each part, the whole-field model of coupling cooling system is developed into a model based on the PCM unit. In this way, the problems of large number of grids and long calculation time are solved, which greatly reduce the computational difficulty and save the computer time.

To sum up, this paper presents a new cooling method of PCM combined with PBE, which solves the problems of large demand of PCM and small operating temperature range at the same time. This method meets the requirements of safety, no power, stability and reliability under special environment and widens the application range of LHTES system for temperature control.

Moreover, the coupling cooling method is analyzed in theoretical and numerical methods. The results of this paper can not only help the establishment of heat transfer model of SR and building containing non-shape-stabilized PCM unit, but also provide reference for analysis and optimization of coupling cooling system in next step.

Acknowledgements

Authors would like to thank the project of the National Natural Science Foundation of China entitled “A study of the characteristics of the surrounding rock cold storage-phase-change heat storage coupling cooling system for mine refuge chambers” (NO. 51378426) and the Youth Science and Technology Innovation Team of Sichuan Province of Building Environment and Energy Efficiency (No. 2015TD0015) for the financial support for this study.

References

[1] Zujing Zhang, Yanping Yuan, Kequan Wang, et al. Experimental investigation on Influencing Factors of air curtain systems barrier efficiency for mine refuge chamber [J]. Process Safety and Environmental Protection. 2016,102:534-546.

[2] Xueqiu He, Li Song. Status and future tasks of coal mining safety in China [J]. Safety Science. 2012, 50:894-898.

[3] Qinjun Lv. Situation and Improvement Measures of the Safe Production of Coal Mines [J]. Energy and Energy Conservation. 2015, 115(4):63-64.(IN CHINESE)

[4] Van Rensburg A.J., Russell H.M.S., Rust H., et al. Functional performance of formal gold mine and colliery refuge bays with special reference to air supply failure [J]. Journal of the Mine Ventilation Society of South Africa. 1988,41(5):58-70.

[5] Mingbo Piao, Jun Mao, Tiejun Wang. Status quo and prospect of the development for underground coal mine refuge chamber [J]. Journal of Coal Science & Engineering. 2013,19(1):38-45.

[6] Junling Yang, Luwei Yang, Juan Wei, et al. Study on open-cycle carbon dioxide refrigerator for movable mine refuge chamber [J]. Applied Thermal Engineering. 2013,52:304-312.

[7] Rick Brake, Graham Bates. Criteria For The Design Of Emergency Refuge Stations For An Underground Metal Mine [J]. AusIMM Proceedings. 1999,304(2):1-12.

[8] Yanxiang Jia, Yingshu Liu, Shufeng Sun, et al. Refrigerating characteristics of ice storage capsule for temperature control of coal mine refuge chamber [J]. Applied Thermal Engineering. 2015,75:756-762.

[9] D. Feldman, D. Banu, D. Hawes, et al. Obtaining an energy storing building material by direct incorporation of an organic phase change material in gypsum wallboard [J]. Solar Energy Materials. 1991, 22:231-242.

[10] Na Zhu, Pengpeng Liu, Pingfang Hu, et al. Modeling and simulation on the performance of a novel doubleshape-stabilized phase change materials wallboard [J]. Energy and Buildings. 2015, 107:181-190.

[11] Camila Barreneche, Lidia Navarro, Alvaro de Gracia, et al. In situ thermal and acoustic performance and environmental impact of the introduction of a shape-stabilized PCM layer for building applications [J]. Renewable Energy. 2016,85:281-286.

[12] Xu Wang, Hang Yu, Lu Li, et al. Research on temperature dependent effective thermal conductivity of composite-phase change materials (PCMs) wall based on steady-state method in a thermal chamber [J]. Energy and Buildings. 2016, 126:408-414.

[13] Ming Zhao, Tingting Zhu, ChangningWang, et al. Numerical simulation on the thermal performance of hydraulic floor heating system with phase change materials [J]. Applied Thermal Engineering. 2016, 93:900-907.

[14] Amitha Jayalath, Lu Aye, Priyan Mendis, et al. Effects of phase change material roof layers on thermal performanceof a residential building in Melbourne and Sydney [J]. Energy and Buildings. 2016, 121:152-158.

[15] G. Hed, R. Bellander. Mathematical modeling of PCM air heat exchanger [J]. Energy and Buildings. 2006, 38:82-89.

[16] Dongliang Zhao, Gang Tan. Numerical analysis of a shell-and-tube latent heat storage unit with fins for air-conditioning application [J]. Applied Energy. 2015, 138:381-392.

[17] H. Benli. Energetic performance analysis of a ground-source heat pump system with latent heat storage for a greenhouse heating. Energy Conversation and Management. 2011, 52(1):581-589.

[18] S. Bouadila，M. Lazaar，S. Skouri, et al. Assessment of the greenhouse climate with a new packed-bed solar air heater at night, in Tunisia. Renewable & Sustainable Energy Reviews. 2014, 35:31-41.

[19] S. Kooli, S. Bouadila, M. Lazaar, et al. The effect of nocturnal shutter on insulated greenhouse using a solar air heater with latent storage energy. Solar Energy. 2015, 115:217-228.

[20] Atyah Najjar, Afif Hasan. Modeling of greenhouse with PCM energy storage [J]. Energy Conversion and Management. 2008,49:3338-3342.

[21] S. S. Bharadwaj, N. K. Bansal. Temperature Distribution Inside Ground for Various Surface Conditions [J]. Building and Environment. 1981, 16(3):183-192.

[22] Yimin Xiao, Xichen Liu, Rongrong Zhang. Calculation of transient heat transfer through the envelope of an underground cavern using Z-transfer coefficient method [J]. Energy and Buildings. 2012, 48:190-198.

[23] A.D.S. Gillies, P. Creevy, G. Danko, et al. Determination of the in situ mine surface heat transfer coefficient[C]// Proceedings of Fifth US Mine Ventilation Symposium. 1991:288-298.

[24] Chenghua Gao, Ruyun Ma. Eigenvalues of discrete Sturm–Liouville problems with eigenparameter dependent boundary conditions [J]. Linear Algebra and its Applications. 2016, 503:100-119.

[25] Yuan Zhang. Transient Temperature Field of Surrounding Rock of the High Geothermal Roadway and Its Heat Control Mechanism by Heat Insulation [D]. China University of Mining and Technology, Beijing, 2013.(IN CHINESE)

[26] Zhenqian Chen, Dongyan Gao, Juan Shi. Experimental and numerical study on melting of phase change materials in metal foams at pore scale [J]. International Journal of Heat and Mass Transfer. 2014,72:646-655.

[27] Guosheng Dai. Heat transfer [M]. Higher Education Press, Beijing, 1999. (IN CHINESE)

[28] Eric Tumilowicz, Cho Lik Chan, Li Pei-wen, et al. An enthalpy formulation for thermocline with encapsulated PCM thermal storage and benchmark solution using the method of characteristics [J]. International Journal of Heat and Mass Transfer. 2014,79:362-377.

[29] Babak Kamkari, Hossein Shokouhmand. Experimental investigation of phase change material melting in rectangular enclosures with horizontal partial fins [J]. International Journal of Heat and Mass Transfer .2014,78: 839-851.

Nomenclature

a	thermal diffusivity, m^2/s
A	calculation accuracy
A_{mush}	fuzzy zone constant
B/C/D	constant number
c_P	specific heat, J/(kg·K)
e	the base of natural logarithms
E	simplified calculation coefficient
f	melt fraction
g	acceleration of gravity,m/s^2
h	convective heat transfer coefficient, $W/(m^2·K)$
h'	enthalpy, J/kg
H	high, m
J	Bessel function of the first kind
l	feature size, m
L	length, m
m	the times of sums
N	number
q	heat flux, W
Q	heat, J
r	radius, m
S	area, m^2; source term
t	temperature, K
u	velocity, m/s
v	velocity, m/s
V	volume, m^3
W	width, m
Y	Bessel function of the second kind

Greek symbols

α	expansion coefficient
β	compute number, m^{-1}
δ	thickness
Δ	difference
ε	constant number
η	correction factor
λ	thermal conductivity, W/(m·K)
ρ	density, kg/m^3
τ	time, s
υ	viscosity, m^2/s

Subscripts

a air
b Buoyancy term
c control heat circle
exp experimental result
f flow air
i inner/indoor
l limited
m melt
o outer
s solidification
t test
w wall
x *x* direction
y *y* direction
0 initial value

Abbreviation

CFD Computational Fluid Dynamics
LHTES Latent Heat Thermal Energy Storage
PBE Precooling the Building Envelope
PCM Phase Change Material
PRESTO Pressure staggering option
SR Surrounding Rock
SIMPLE Semi-Implicit Method Pressure Linked Equation
TES Thermal energy storage
TTM temperature transforming model
UDF User Define Function

Dimensionless numbers

Bi Biot number
Fo Fourier number
Gr Grashof number
Nu Nusselt number
Pr Prandtl Number
R_c the dimensionless radius of control heat circle
Γ the dimensionless radius
Θ the dimensionless temperature
Φ the dimensionless radius of far boundary
Ψ_m the dimensionless radius of inner wall